



Magnetic resonance imaging of the static magnetic field distortion caused by magnetic nanoparticles: Simulation and experimental verification



Daniel Gogola*, Oliver Štrbák, Andrej Krafčík, Martin Škrátek, Ivan Frollo

Institute of Measurement Science, Slovak Academy of Sciences, Bratislava, Slovakia

ARTICLE INFO

Article history:

Received 25 June 2014
 Received in revised form
 28 September 2014
 Accepted 3 October 2014
 Available online 18 October 2014

Keywords:

Magnetic nanoparticles
 Contrast agents
 Magnetic fields
 MRI
 Magnetic dipoles
 Magnetic thin layer
 Molecular double layer

ABSTRACT

Magnetic nanoparticles are widely used as a contrast agent in magnetic resonance imaging (MRI). Nanoparticles in contrast agents possess a magnetic moment which generates local inhomogeneities in the static magnetic field of the MR scanner. These inhomogeneities cause a rapid loss of phase coherence which leads to the fast decay of the MR signal and thus produce a negative contrast in MR images. This article is focused on the interaction of magnetic nanoparticles aligned in a thin layer with the external homogeneous magnetic field, which changes the uniform distribution of magnetic nanoparticles in the carrier liquid. The goal of this study is to investigate the influence of the arrangement of magnetic nanoparticles on the final image contrast during MRI.

© 2014 Elsevier B.V. All rights reserved.

1. Introduction

Magnetic nanoparticles have been gradually gaining importance in clinical medicine as contrast agent for MRI liver diagnostics [1–3], as therapeutic agent for magnetic hyperthermia [3] or as transport agent for drug delivery to the site of interest in the human body [4,5]. Nowadays, magnetic nanoparticles have also found application in many other research areas, such as target biological entities, the magnetic separation of cells, and MRI, cancer therapy [6–10].

In general, magnetic nanoparticles consist of a solid core, most often of spherical shape. The solid core of the nanoparticle may consist of iron powder or substances containing Fe^{2+} or Fe^{3+} ions. A typical example is magnetite or maghemite. Unfortunately, the Fe^{2+} form is very toxic. Therefore, a surface treatment for each individual application is required. The surface treatment forms a chemically active coat, which can provide bindings with other molecules of interest.

For medical (in-vivo) applications the magnetic nanoparticles must be coated with biocompatible polymers such as dextran, protein, polyvinyl alcohol or polyethylene glycol. These polymers allow the binding of genes or various drugs by covalent

attachment [11]. This functionality of magnetic nanoparticles allows their use for diverse applications including tumour treatment by magnetic hyperthermia [4,12], the delivery of chemotherapeutic or radioactive drugs, the improved delivery of peptides for gene transfer [12], thrombolysis, detoxification of blood, delivery of local anaesthesia or neuroblockers [13].

Another functionality which can influence the applicability of the magnetic nanoparticles is their size. Depending on their hydrodynamic diameter they can be classified into two groups, namely superparamagnetic iron oxide nanoparticle (SPION) with a diameter greater than 50 nm, or ultra-small superparamagnetic iron oxide nanoparticle (USPIO) with a diameter lower than 50 nm [1,14]. Superparamagnetism occurs when the particle is small enough to behave as a single dipole.

The shape of the hysteresis curve is in direct relation to the properties of magnetic materials such as saturation magnetization, maximum hysteresis loss and size of magnetic particles [15].

The interaction of the planar electromagnetic phantom, or the weak magnetic materials of the various shapes with homogeneous static magnetic field, was described and mathematically modelled in [16,17]. The magnetic field distribution in these articles was calculated as the superposition of elementary areas, as opposed to this study where magnetic field distribution was calculated as a superposition of individual magnetic domains.

* Corresponding author.

E-mail address: daniel.gogola@savba.sk (D. Gogola).

Magnetic properties of the single nanoparticle Fe_3O_4 , with size 10 nm, were simulated and discussed in [18]. The magnetic field distribution of the group of nanoparticles was simulated using the equations published in [19].

The aim of this study was to investigate the influence of magnetic nanoparticle distribution in MR images, and to help understand the artefacts typical in liver or kidney MR imaging. We analysed the magnetic field of the near surroundings of the groups of magnetic nanoparticles Fe_3O_4 , which are regarded as small magnetic dipoles.

2. Materials and methods

2.1. Simulations

To calculate the magnetic field of each particle in the near surroundings, a cube with the size of $20 \times a$ was selected, where a is the particle diameter, in our case 10 nm. A simulated magnetic particle is situated in the centre of each cube. The magnetic field distribution was simulated in a Matlab environment (version R2011b, Mathworks Inc., USA), using equations as described in the Appendix. In our study we used four nanoparticles, which were evenly spaced between each other. In each simulation, the

distance between the particles was evenly incremented (Fig. 1). For each inter-particle distance of four nanoparticles a profile of magnetic field was observed. This profile was selected as shown in Fig. 1.

2.2. MR experiments

On the basis of the simulation we carried out the experiments on an ESAOTE Opera MR scanner. A **sensitivity test** was performed by the quantification of image intensity at ESAOTE Opera. We used a dedicated home-made phantom (Fig. 3). The phantom consisted of a series of Eppendorf tubes (1.5 ml volume), filled with the different concentrations of magnetic nanoparticles suspended in distilled water. The active substance of the phantoms was represented by water-based ferrofluid Type: EMG 607, made by FerroTec Corporation (Santa Clara, California, USA). The purpose of this test was to understand the low limit of the nanoparticle concentration which can be distinguished in the MR image.

In all cases we studied static magnetic field distribution, which was higher than the smallest induced magnetic field observable with the MR scanner. The smallest observable influence of the magnetic field is the magnetic polarization \mathbf{J} , generated by the nanoparticles placed in external field \mathbf{B}_0 , which causes observable loss of the signal in MRI. Magnetic polarization of particle \mathbf{J} can be

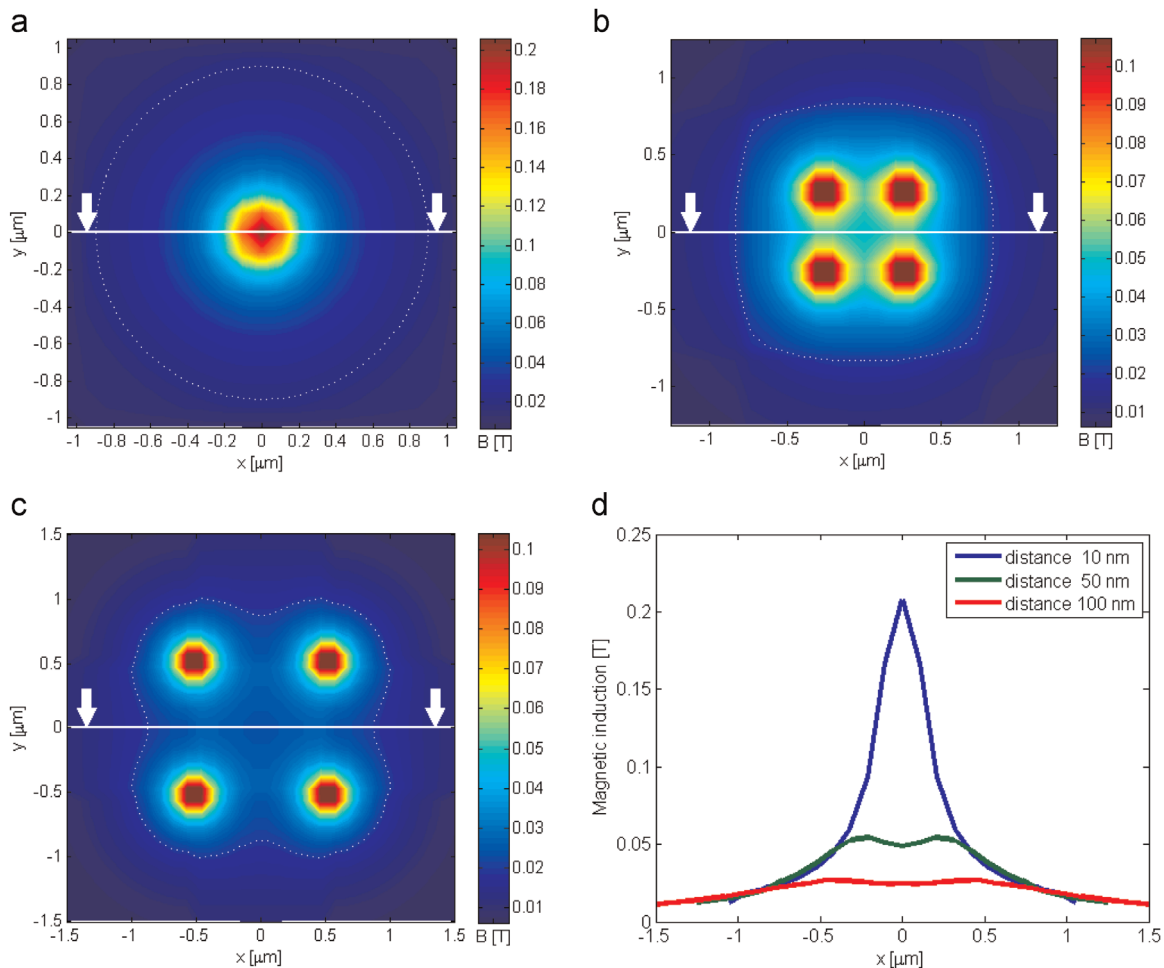


Fig. 1. Contour plot of the magnetic field of four nanoparticles. Dotted isolines define the magnetic field with value ≥ 0.02 T. (a) The centre-to-centre distance of nanoparticles was 10 nm, what cause that individual nanoparticles cannot be distinguished. Diameter of contour with value of magnetic field 0.02 T is 170 nm. (b) The centre-to-centre distance of nanoparticles was 50 nm. Diameter of contour with value of magnetic field 0.02 T is 160.3 nm. (c) The centre-to-centre distance of nanoparticles was 100 nm. Diameter of contour with value of magnetic field 0.02 T is 168 nm. (d) Profile of magnetic field in selected line. White arrows depict the line where the profile of contour plot was measured.

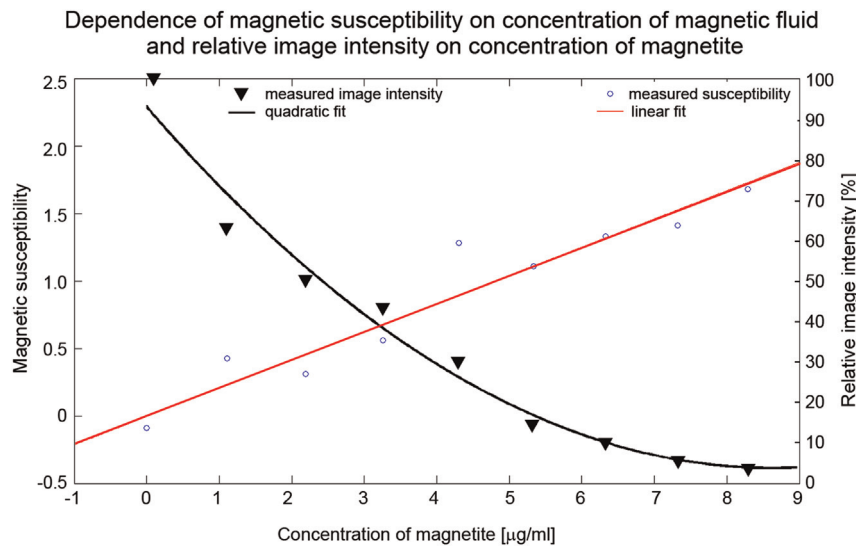


Fig. 2. Dependence of signal intensity on the concentration of magnetite and relative image intensity on concentration of magnetite. As reference, (maximal) value of signal in distilled water was chosen. Other phantom solutions are normalized to distilled water expressed by the percentage.

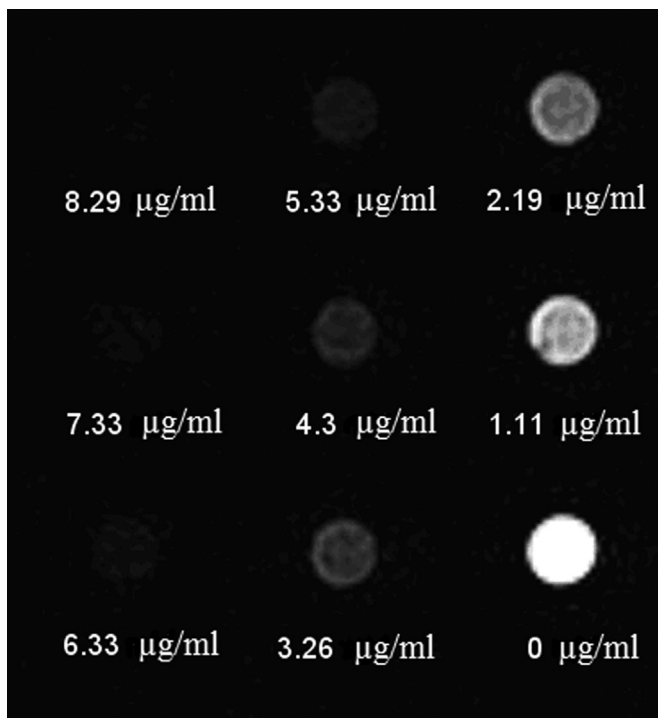


Fig. 3. Image of nine home-made phantoms which show gradual decay of signal intensity due to an increased concentration of magnetic nanoparticles in samples [23].

calculated using equation (1) [19,20]:

$$\mathbf{J} = \chi \mathbf{B}_0 \quad (1)$$

where χ is the volume magnetic susceptibility, and \mathbf{B}_0 is a vector of the external magnetic field.

The change of homogeneous magnetic field \mathbf{B}_0 in the area where the magnetic nanoparticle is placed is expressed by the following equation:

$$\mathbf{B} = \mathbf{B}_0 + \mathbf{J} \quad (2)$$

where \mathbf{B} is a vector of the total magnetic field,

Volume magnetic susceptibility (with value close to initial magnetic susceptibility) of each sample in phantom was measured by the Superconducting Quantum Interference Device (SQUID) magnetometer with a frequency of 2.8 Hz and magnetising field of 0.29 mT [21,22].

For the first experiment, the magnetic water-based ferrofluid EMG 607 was placed into the Teflon capillary which had a diameter of 1.2 mm and a volume of 11.3 μl . Another identical Teflon capillary was left empty (filled with air) for comparison. The space around the capillaries was filled with the solution consisting of a 5 mM NiCl_2 and 55 mM NaCl dissolved in the distilled water. The wall thickness of the Teflon capillaries was 0.1 mm.

The sample was placed vertically into an MR scanner and imaged by the gradient echo sequence with TE/TR 14/2400 ms, acquisition matrix 256×192 , FOV 256×256 , acquisition time 11 min 15 s, MR acquisition type 2D, flip angle 65, nominal resolution $1.0 \times 1.33 \text{ mm}^2$, number of slices 1 and slice thickness 2 mm. The purpose of this test was to quantify the influence of the water-based ferrofluid concentration on the resulting diameter of the image artefact.

For the second experiment, 1% agar gel (Haihang Industry Co., Shandong, China (Mainland)), mixed with distilled water was prepared. After solidification, two cylinders with diameter 26 mm and height 12 mm have been cut from the gel. In this experiment the magnetic water-based ferrofluid EMG 607, with the same volume (11.3 μl), was placed on the surface of filter paper F261 (Fisher Scientific, Germany) and left free to soak into this filter paper. The producer of water-based ferrofluid EMG 607 indicated that the initial magnetic susceptibility was 1.63 SI and the concentration of magnetite was 2% by volume.

The filter paper with applied magnetic water-based ferrofluid EMG 607 was placed between two cylinders from the agar gel. This sample was placed into the MR scanner and the measurement was performed in coronal plane by the gradient echo sequence, TE/TR 14/2400 ms, acquisition matrix size 256×192 , FOV 256×256 , nominal resolution $1.33 \times 1.0 \text{ mm}$, total measurement time 12 min 14 s, MR acquisition type 2D, flip angle 90° and slice thickness 2 mm (Fig. 4).

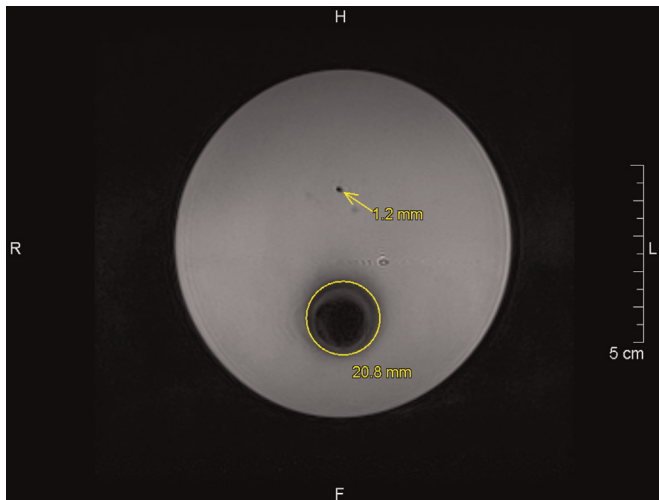


Fig. 4. MRI of two capillaries: at the top is shown the capillary without ferrofluid with a diameter 1.2 mm, at the bottom is shown an identical capillary filled with water-based ferrofluid EMG 607. The significant difference of the diameters of the resulting structures is shown in the image.

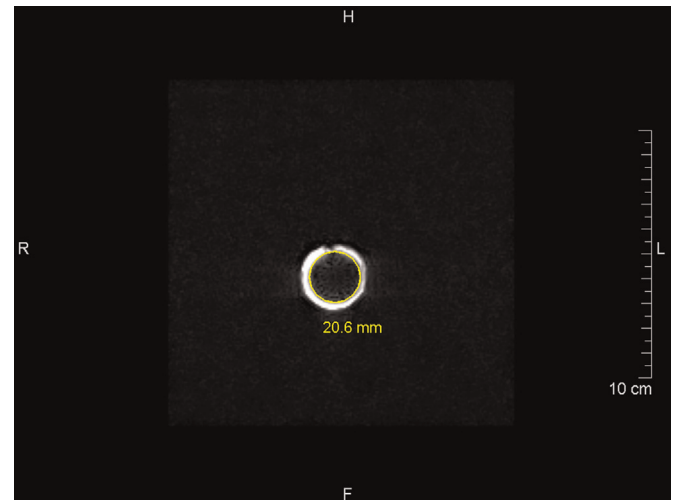


Fig. 5. MR image of gel cylinders and filter paper with soaked magnetic liquid EMG 607. The diameter of inhomogeneity, caused by filter paper with EMG 607, was 20.6 mm.

Table 1
Description properties of used phantoms

Phantom consist of	Concentration of EMG607 [$\mu\text{g/ml}$]	Volume magnetic susceptibility of phantom (SI)	T2 relaxation time [ms]
distilled water	0	-9.04×10^{-6}	1800 ± 20
distilled water+EMG607	1.11	4.24×10^{-5}	31.0 ± 0.3
	2.19	3.11×10^{-5}	15.2 ± 0.2
	3.26	5.58×10^{-5}	10.0 ± 0.079
	4.3	1.28×10^{-4}	8.8 ± 0.088
	5.33	1.11×10^{-4}	6.4 ± 0.073
	6.33	1.33×10^{-4}	5.2 ± 0.052
	7.32	1.41×10^{-4}	4.6 ± 0.053
	8.29	1.68×10^{-4}	4.1 ± 0.05

3. Results and discussion

3.1. Simulations

The simulation determines the shape of the magnetic field generated by the magnetic nanoparticles in their close surroundings, for three centre-to-centre distances (10, 50 and 100 nm). For the purpose of these experiments, we identified isolines with the magnetic field intensity equal to 0.02 T. The results of the simulations surprisingly show that the change of area delineated by isolines was lower than 10 nm. The diameter of the outside contour with magnetic field intensity 0.02 T was approximately $170 \text{ nm} \pm 10 \text{ nm}$ (Fig. 1) in all 3 experiments (centre-to-centre distances of nanoparticles of 10, 50 and 100 nm). This change corresponds to the size of a single magnetic nanoparticle.

In the simulations, the inter-particle distance was 10 nm (Fig. 1a) or 50 nm (Fig. 1b) or 100 nm (Fig. 1c), Corresponding magnetic induction in the centre between four nanoparticles was 200 mT, 45.5 mT and 24 mT respectively.

3.2. MR experiments

Based on the simulations we performed **sensitivity test** experiments in an MR scanner 0.178 T ESAOTE Opera (Esaote S.p.A., Genoa, Italy). We measured a series of Eppendorf tubes, as described above (Fig. 3). We identified the centrally positioned tube of the phantom as the one with the lowest intensity, which can be

seen in the image. This Eppendorf tube was subsequently measured using SQUID and the susceptibility was evaluated. Based on equation (1), we calculated that the magnetic polarization J which is observable in our scanner is equal to $9.93 \mu\text{T}$.

Phantom parameters and corresponding susceptibilities and T2 relaxation time values are summarised in Table 1. The decrease in **signal intensity** depending on the concentration of used contrast agent is shown in (Fig. 2). The dependence of **magnetic susceptibility** on the concentration of magnetic nanoparticles in each sample is linear, as shown in Fig. 2.

Two artefacts are shown in Fig. 4. Upper (small) artefact caused by the air resulted in a black area 1.2 mm in diameter. The lower artefact caused by the susceptibility of magnetic fluid EMG 607 causes a black circle with a diameter of 20.8 mm.

Our MRI experiments have shown that the same volume of magnetic nanoparticles both in aggregate state (Fig. 4) and in planar shape (Fig. 5) can cause, in the studied plane, an artefact of the same diameter. Artefact diameter in both experiments (aggregate state and in planar shape), revealed a difference of 0.2 mm at a nominal resolution of 0.547 mm/pixel. The experimental results confirm the simulations. The outer diameter of the nanoparticle-induced artefact was the same for both states, aggregate and planar.

4. Conclusion

We have presented a theoretical simulation of the magnetic field variation caused by a thin layer of magnetite nanoparticles. The result of this simulation was compared with an experiment which was carried out on a clinical MRI scanner with vertical orientation of the basic magnetic field B_0 . The simulation and experiment showed that by using the contrast media it is possible to evaluate the concentration or susceptibility of the particles in thin layer but not their distribution in this layer.

Acknowledgments

This work was supported by the Slovak Scientific Grant Agency VEGA 2/0090/11 and by Slovak Research and Development Agency APVV-0431-12.

Appendix

The following expressions were used for the simulation of magnetic field distribution which was generated by the group of magnetic nanoparticles.

The analytic expressions for the magnetic field of a circular current loop in Cartesian coordinates adjusted to a cube-shaped particle are:

$$B_x = xz \frac{\mu_0 \vec{\mu}_{mag}}{12\pi a^2} C_1 \quad B_y = yz \frac{\mu_0 \vec{\mu}_{mag}}{12\pi a^2} C_1 \quad B_z = \frac{\mu_0 \vec{\mu}_{mag}}{12\pi a^2} C_2$$

where μ_{mag} is the particle magnetic moment, μ_0 is permeability, and a is the particle size. The following substitutions are used for simplicity: $C_1 = [(\alpha^2 + r^2)E(k^2) - \alpha^2 K(k^2)] / 2\alpha^2 \beta \rho^2$ and $C_2 = [(\alpha^2 - r^2)E(k^2) + \alpha^2 K(k^2)] / 2\alpha^2 \beta$, where $\rho^2 = x^2 + y^2$, $r^2 = x^2 + y^2 + z^2$, $\alpha^2 = a^2 + r^2 - 2a\rho$, $\beta^2 = a^2 + r^2 + 2a\rho$, $k^2 = 1 - \alpha^2/\beta^2$. $K(k^2)$ and $E(k^2)$ are the elliptic integrals of the first and second kind. In this approach, the nanoparticle is regarded as a magnetic dipole with defined magnetic moment μ and approximated to the current loop.

References

- [1] A. Bjørnerud, L. Johansson, The utility of superparamagnetic contrast agents in MRI: theoretical consideration and applications in the cardiovascular system, *NMR Biomed.* 17 (2004) 465–477.
- [2] Y.-X. Wang, S.M. Hussain, G.P. Krestin, Superparamagnetic iron oxide contrast agents: physicochemical characteristics and applications in MR imaging, *Eur. Radiol* 11 (2001) 2319–2331.
- [3] A. Ba-Ssalamah, N. Fakhrai, W.K. Matzek, A.M. Herneth, A. Stadler, N. Bastati, C. J. Herold, W. Schima, Magnetic resonance imaging of liver malignancies, *Top Magn. Reson. Imaging* 18 (6) (2007) 445–455.
- [4] M. Johannsen, U. Gneveckow, L. Eckelt, A. Feussner, N. Waldöfner, R. Scholz, S. Deger, P. Wust, S.A. Loening, A. Jordan, Clinical hyperthermia of prostate cancer using magnetic nanoparticles: presentation of a new interstitial technique, *Int. J. Hyperther.* 21 (7) (2005) 637–647.
- [5] J. Xie, S. Lee, X. Chen, Nanoparticle-based theranostic agents, *Adv. Drug Deliv. Rev.* 62 (2010) 1064–1079.
- [6] B. Shapiro, Towards dynamic control of magnetic fields to focus magnetic carriers to targets deep inside the body, *J. Magn. Magn. Mater.* 321 (10) (2009) 1594.
- [7] S.A. Khashan, E. Elnajjar, Y. Haik, CFD simulation of the magnetophoretic separation in a microchannel, *J. Magn. Magn. Mater.* 323 (23) (2011) 2960–2967.
- [8] I. Šafařík, M. Šafaříková, Use of magnetic techniques for the isolation of cells, *J. Chromatogr. B Biomed. Sci. Appl* 722 (1999) 33–53.
- [9] Z. Ma, H. Liu, Synthesis and surface modification of magnetic particles for application in biotechnology and biomedicine, *China Part 5* (2007) 1–10.
- [10] F. Scherer, M. Anton, U. Schillinger, J. Henke, C. Bergemann, A. Krüger, B. Gänsbacher, C. Plank, Magnetofection: enhancing and targeting gene delivery by magnetic force in vitro and in vivo, *Gene Ther.* 9 (2) (2002) 102–109.
- [11] R.V. Mehta, R. Desai, P. Bhatt, R.V. Upadhyay, Synthesis and characterization of certain nanomagnetic particles coated with citrate and dextran molecules, *Indian J. Pure Ap. Phy* 44 (2006) 537–542.
- [12] A. Doagă, C.P. Constantin, A. Cojocariu, I. Astefanoaei, I. Dumitru, O.F. Caltun, Phenomenological study of thermal field generated by nanoparticles arrays in hyperthermia as treatment method, *J. Adv. Res. Phys.* 2 (1) (2011) 166–168.
- [13] O. Veisoh, J.W. Gunn, M. Zhang, Design and fabrication of magnetic nanoparticles for targeted drug delivery and imaging, *Adv. Drug Deliv. Rev.* 62 (2010) 284–304.
- [14] U.O. Häfeli, M.A. Lobedann, J. Steingroewer, L.R. Moore, J. Riffle, Optical method for measurement of magnetophoretic mobility of individual magnetic microspheres in defined magnetic field, *J. Magn. Magn. Mater.* 293 (2005) 224–239.
- [15] P. Majewski, B. Thierry, Functionalized magnetite nanoparticles – synthesis, properties, and bio-applications, *Crit. Rev. Solid State* 32 (2007) 203–215.
- [16] R.P. Feynman, R.B. Leighton, M. Sands, *The Feynman Lectures on Physics*, Addison-Wesley Publishing Company, 1966.
- [17] I. Frollo, P. Andris, D. Gogola, J. Příbil, L. Valkovič, P. Szomolányi, Magnetic field variations near weak magnetic materials studied by magnetic resonance imaging techniques, *IEEE Trans. Magn* 8 (2012) 2334–2339.
- [18] I. Frollo, P. Andris, J. Příbil, L. Vojtišek, T. Dermek, L. Valkovič, Measurement and imaging of planar electromagnetic phantoms based on NMR imaging methods, *Meas. Sci. Rev* 10 (3) (2010) 97–101.
- [19] O. Štrbák, P. Kopčanský, M. Timko, I. Frollo, Single biogenic magnetite nanoparticle physical characteristics – a biological impact study (for MagMeet 2012 participants), *IEEE Trans. Magn.* 49 (1) (2013) 457–462.
- [20] P. Cicmanec, *Basic Physics 2: Electricity and Magnetism*, ALFA, Bratislava, 1980 (in Slovak).
- [21] V. Zrubec, A. Cigáň, J. Maňka, Simplified fast method for magnetic characteristics measurement of the HTc superconducting materials, *Phys. C: Superconduct.* 223 (1–2) (1994) 90–94.
- [22] y. Citacia, M. Škrátek, I. Šimáček, A. Dvurečenskij, M. Majerová, J. Maňka, Magnetometric measurements of low concentration of coated Fe₃O₄ nanoparticles, *Acta Phys. Pol. A* 126 (2014) 396–397.
- [23] D. Gogola, A. Krafčík, O. Štrbák, I. Frollo, Magnetic resonance imaging of surgical implants made from weak magnetic materials, *Meas. Sci. Rev* 13 (4) (2013) 165–168.